Carbohydrate Polymers 91 (2013) 419–427

Contents lists available at SciVerse ScienceDirect

Carbohydrate Polymers

journal homepage: www.elsevier.com/locate/carbpol

Carbon nanotube-incorporated multilayered cellulose acetate nanofibers for tissue engineering applications

Yu Luo[a], Shige Wang[b], Mingwu Shen[a,*], Ruiling Qi[c], Yi Fang[a], Rui Guo[a], Hongdong Cai[b], Xueyan Cao[a], Helena Tomás[d], Meifang Zhu[b], Xiangyang Shi[a,d,*]

[a] College of Chemistry, Chemical Engineering and Biotechnology, Donghua University, Shanghai 201620, People's Republic of China
[b] State Key Laboratory for Modification of Chemical Fibers and Polymer Materials, Donghua University, Shanghai 201620, People's Republic of China
[c] College of Textiles, Donghua University, Shanghai 201620, People's Republic of China
[d] CQM – Centro de Química da Madeira, Universidade da Madeira, Campus da Penteada, 9000-390 Funchal, Portugal

ARTICLE INFO

Article history:
Received 24 March 2012
Received in revised form 11 August 2012
Accepted 19 August 2012
Available online 25 August 2012

Keywords:
Self-assembly
Carbon nanotube
Electrospinning
Nanofiber
Cell culture

ABSTRACT

We report the fabrication of a novel carbon nanotube-containing nanofibrous polysaccharide scaffolding material via the combination of electrospinning and layer-by-layer (LbL) self-assembly techniques for tissue engineering applications. In this approach, electrospun cellulose acetate (CA) nanofibers were assembled with positively charged chitosan (CS) and negatively charged multiwalled carbon nanotubes (MWCNTs) or sodium alginate (ALG) via a LbL technique. We show that the 3-dimensional fibrous structures of the CA nanofibers do not appreciably change after the multilayered assembly process except that the surface of the fibers became much rougher than that before assembly. The incorporation of MWCNTs in the multilayered CA fibrous scaffolds tends to endow the fibers with improved mechanical property and promote fibroblast attachment, spreading, and proliferation when compared with CS/ALG multilayer-assembled fibrous scaffolds. The approach to engineering the nanofiber surfaces via LbL assembly likely provides many opportunities for new scaffolding materials design in various tissue engineering applications.

1. Introduction

Tremendous progress has been witnessed in the development of various tissue engineering scaffolding materials since the pioneering work reported by Langer and Vacanti in 1990s (Langer & Vacanti, 1993, 1999). In the field of tissue engineering, design of suitable bioactive scaffold materials that can mimic the extracellular matrices (ECM) is an essential prerequisite (Harrington et al., 2006). Much effort has been devoted to fabricate such scaffold materials for improved cellular attachment, proliferation, and differentiation (Abraham, Riggs, Nelson, Lee, & Rao, 2010; Rowley, Madlambayan, & Mooney, 1999; Sottile, 2004; Wei & Ma, 2008).

Electrospinning is a simple and versatile technique that can be used to fabricate fibers with a diameter ranging from tens of nanometers to a few microns (Reneker & Chun, 1996). The fabricated nanofibrous mats with ultra-fine fiber diameter, high surface area to volume ratio, three-dimensional (3D) porous structure can well mimic the natural ECM (Bhattarai, Li, Edmondson, & Zhang, 2006; Huang et al., 2010; Li, Laurencin, Caterson, Tuan, & Ko, 2002; Li et al., 2005; Mo, Xu, Kotaki, & Ramakrishna, 2004; Yoshimoto, Shin, Terai, & Vacanti, 2003), providing a useful option for tissue engineering applications. For practical biomedical applications, the formed nanofibrous mats have to be functionalized to improve the surface physicochemical properties, mechanical durability, biocompatibility, and cellular response.

As one of the most important surface modification techniques, layer-by-layer (LbL) self-assembly has been widely utilized to deposit multilayers onto planar substrates (Decher, 1997; Mamedov & Kotov, 2000; Olek et al., 2004; Schlenoff & Decher, 2003) or nanofiber surfaces (Almodóvar & Kipper, 2011; Deng et al., 2010, 2011; Mamedov & Kotov, 2000; Xiao et al., 2009). For improved cellular functionalities of planar substrates, Yang et al. reported the formation of hydrogen-bonded multilayers comprised of polyacrylamide and a weak polyelectrolyte, such as poly(acrylic acid) or poly(methacrylic acid) that have a high resistance to the adhesion (cytophobicity) of mammalian fibroblasts (Yang, Mendelsohn, & Rubner, 2003). Likewise, poly(glutamic acid) and poly(L-lysine) multilayers have been successfully self-assembled on planar substrates (Halthur & Elofsson, 2004; Lavalle et al., 2002) and display very good biocompatibility for implant coatings (Picart et al., 2005). In another study, Caruso and coworkers reported the

* Corresponding authors at: 2999 North Renmin Road, College of Chemistry, Chemical Engineering and Biotechnology, Donghua University, Shanghai 201620, People's Republic of China. Tel.: +86 21 67792656; fax: +86 21 67792306 804.
E-mail addresses: mingwu_shen@yahoo.com (M. Shen), xshi@dhu.edu.cn (X. Shi).

0144-8617/$ – see front matter © 2012 Elsevier Ltd. All rights reserved.
http://dx.doi.org/10.1016/j.carbpol.2012.08.069

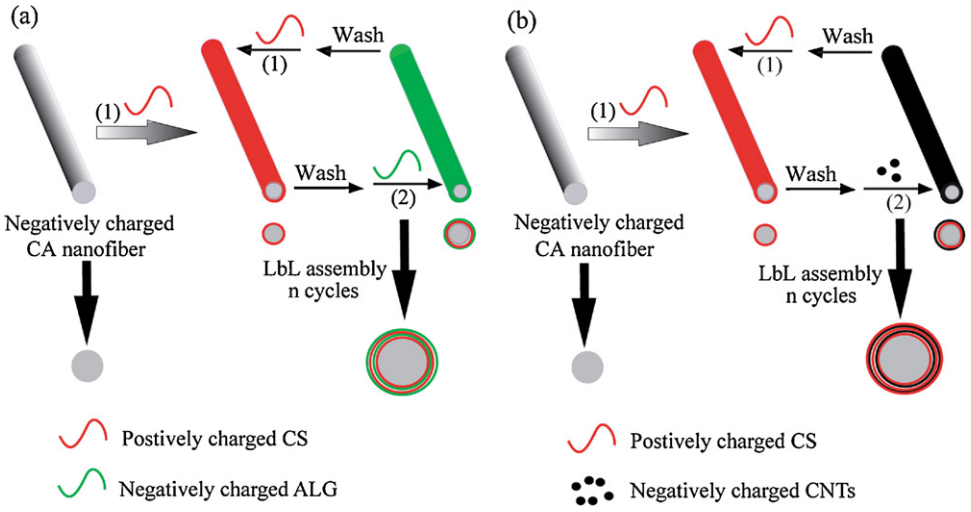

Fig. 1. Schematic illustration of the preparation of multilayered CA/(CS/MWCNTs)$_n$ and CA/(CS/ALG)$_n$ scaffolds.

construction of peptide-functionalized, low-biofouling click multilayers for promoting cell adhesion and growth (Kinnane, Wark, Such, Johnston, & Caruso, 2009). For the fiber surface functionalization, Deng et al. reported the construction of chitosan (CS) and alginate (ALG) multilayers onto cellulose acetate (CA) nanofibers for cell culture. These studies clearly suggest that the LbL self-assembly technique can be used to modify either planar substrates or fiber surfaces to improve the cellular functionalities.

In our previous work, we have shown that incorporating multiwalled carbon nanotubes (MWCNTs) within the electrospun polymer nanofibers is able to promote protein adsorption onto the fibrous substrates, significantly regulating the cellular spreading and proliferation (Liao et al., 2011; Liu et al., 2010). The improved cellular response is likely due to the presence of MWCNTs in the nanofibers that allows favorable protein adsorption from culture media onto the porous membrane structures (Meng et al., 2009). In our reported work, the MWCNTs were incorporated within the polymer nanofibers by simply electrospinning the polymer solution mixed with the MWCNTs (Liao et al., 2011; Liu et al., 2010). This approach does not allow for precise engineering of the nanofiber surface and the surface chemistry of the fibers cannot be easily regulated. Motivated by the versatile LbL self-assembly approach for fiber surface modification and the unique properties of MWCNTs in regulating cellular growth, we attempted to assemble electrospun CA nanofibers with multilayers of CS and MWCNTs to form a novel nanofiber-based scaffolding material for tissue engineering applications since CS is known to be a biocompatible naturally occurring polysaccharide material (Chicatun et al., 2011).

In this present study, we fabricated the MWCNT-containing nanofibrous polysaccharide scaffolds by combining electrospinning and LbL self-assembly techniques. Electrospun CA nanofibrous mats were first formed and used as templates for subsequent deposition of CS/MWCNTs multilayers via electrostatic self-assembly. For comparison, CS/ALG multilayers were also deposited onto the CA nanofibers (Fig. 1) since ALG is a biocompatible naturally occurring polymer and has been widely used in tissue engineering applications (Zhou & Xu, 2011). The formed multilayered CA nanofibers were characterized by scanning electron microscopy (SEM), Fourier transform infrared spectroscopy (FTIR), thermogravimetric analysis (TGA), and mechanical durability tests. The protein adsorption behavior of the scaffolds was also investigated. Then, the cell attachment and proliferation viabilities onto the nanofibrous scaffolds were evaluated by 3-(4,5-Dimethylthiazol-2-yl)-2,5-diphenyltetrazolium bromide (MTT) assay of cell viability and SEM observation of the cell morphology. Finally, the hemocompatibility of the multilayered CA nanofibrous scaffolds was assessed by hemolysis assay. To our knowledge, this is the first attempt to assemble MWCNTs onto the electrospun nanofiber-based scaffolding materials via an LbL assembly technique for potential tissue engineering applications.

2. Experimental

2.1. Materials

CA (bound acetic acid of 54.5–56.0 wt%, intrinsic viscosity of 300.0–500.0 mPa s), acetone, and CS (medium molecular weight, degree of deacetylation >90%, intrinsic viscosity 50.0–800.0 mPa s) were from Sinopharm Chemical Reagent co., Ltd. ALG with low intrinsic viscosity was from J&K chemical. MWCNTs (diameter 30–70 nm, length 100–400 nm) were obtained according to literature (Petersen, Huang, & Weber, 2008) and were functionalized with carboxyl residues according to a procedure described in literature (Lu & Imae, 2007). In brief, 20 mg of MWCNT was refluxed in 20 mL HNO_3/H_2SO_4 (v/v, 3:1) for 24 h, followed by filtration and drying to render the surface of MWCNTs with carboxylic acid residues. Mouse fibroblasts (L929 cells) were obtained from the Institute of Biochemistry and Cell Biology, the Chinese Academy of Sciences (Shanghai, China). Dulbecco's modified Eagle's medium (DMEM), fetal bovine serum (FBS), penicillin, and streptomycin were purchased from Hangzhou Jinuo Biomedical Technology (Hangzhou, China). Human blood stabilized with heparin was kindly provided by Shanghai First People's Hospital (Shanghai, China). All other chemicals with reagent grade were from Sinopharm Chemical Reagent Co., Ltd. (Shanghai, China). The water used in all the experiments was purified using a Milli-Q Plus 185 water purification system (Millipore, Bedford, MA) with a resistivity higher than 18 MΩ cm.

2.2. Electrospinning of CA nanofibers

CA (12.5 wt%) solution was prepared by dissolving 1.8 g CA powder into 15 mL acetone/N,N-dimethylformamide mixture solvent (2/1, v/v) with vigorous magnetic stirring for 12 h at 25 °C, and the solution was sonicated using a water bath ultrasonic cleaner (50 w, 15 × 14 × 10 cm (length × width × height), SK1200H, Shanghai KUDOS Inc., China) for 30 min before use. Freshly prepared CA solution was loaded into a syringe with a needle having an inner

diameter of 0.8 mm, and the feed rate was controlled by a syringe pump (JZB-1800, Jian Yuan Medical Technology Co., Ltd., China) at 1 mL/h. The high-voltage power supply (BGG40/2, Institute of Beijing High Voltage Technology, China) was connected to the needle by a high-voltage insulating wire with two clamps at the ends. An aluminum board was used as the collector and was connected to the ground. The electrospinning setup can be found in our previous reports (Liao et al., 2011; Liu, Guo, Shen, Wang, & Shi, 2009). The distance of tip to collector was set at 20 cm, and the electrospinning voltage was kept at 20 kV. The temperature and humidity were kept at 25 °C and 40–50%, respectively. The prepared nanofibrous mats were dried for 24 h at 80 °C to remove the trace solvent under vacuum.

2.3. Multilayered self-assembly onto CA nanofibers

The CA mats were hydrolyzed in a 0.05 M NaOH aqueous solution at ambient temperature for 7 d according to a previous report (Deng et al., 2010). This hydrolysis reaction rendered the CA mats with increased density of carboxyl groups, which can be deprotonated in water at a pH of 6.0–6.5 to make the CA mats have surface negative charge, as verified by Rodríguez, Renneckar, and Gatenholm (2011). The CS solution (1 mg/mL) was prepared by dissolving 100 mg CS powder into 1% (v/v) acetic acid solution containing 0.5 M NaCl. The ALG solution (1 mg/mL) was prepared by dissolving 100 mg ALG powder into 100 mL ultrapure water containing 0.5 M NaCl. The MWCNTs suspension (1 mg/mL) was prepared by dispersing 100 mg MWCNTs powder into 100 mL ultrapure water.

CS/MWCNTs multilayers were LbL-assembled onto the fabricated CA nanofibers (Fig. 1). The negatively charged CA nanofibers (Deng et al., 2010) enabled the deposition of positively charged CS as the first layer. In a typical procedure, the CA nanofibrous mats were first immersed into CS solution for 5 min, followed by rinsing with water three times (each rinsing step took 2 min). Then, the substrates were immersed in the negatively charged MWCNTs solution for 5 min, followed by similar rinsing steps in water. The immersion/rinsing cycles were repeated until the desired number of bilayers was achieved. The CS/MWCNTs multilayers thus obtained were denoted as $(CS/MWCNTs)_n$. Similarly, CS/ALG multilayers were also assembled onto the CS nanofibers and were denoted as $(CS/ALG)_n$ (Fig. 1).

2.4. Characterization techniques

The morphology of nanofibrous mats was observed by SEM using a Hitachi TM 1000 scanning electron microscope with an accelerating voltage of 10 kV. The fibrous mats were sputter coated with a 10-nm thick gold film before measurements. Fiber diameters were measured using Image J 1.40 G software (http://rsb.info.nih.gov/ij/down-load.html). At least 300 nanofibers from different SEM images for each sample were randomly selected and analyzed. Zeta-potential measurements were carried out using a Zetasizer Nano ZS system (Malvern, UK) equipped with a standard 633 nm laser. The aqueous solutions of MWCNTs, CS, and ALG with a concentration of 1 mg/mL were measured. The multilayered $CA(CS/ALG)_n$ and $CA(CS/MWCNTs)_n$ nanofibrous mats were characterized by FTIR (Nicolet Nexus 670 FTIR spectrometer). All spectra were recorded in a wavenumber range of 4000–650 cm^{-1}. TGA was performed by TGA Q500 thermogravimetric analyzer (TA instruments, New Castle, DE) under N_2 in the temperature range of 30–800 °C with a heating rate of 48 °C/min. The mechanical properties of nanofibrous mats were measured by a material testing machine (H5K-S, Hounsfield, UK) at 20 °C, relative humidity of 63%, and a stretching speed of 10 mm/min. The electrospun nanofibrous mats before and after self-assembly were punched into small strips with width × gauge length = 10 × 50 mm^2, and five strips from different sites of each fibrous mat sample were chosen for the tensile test. Stress and strain were calculated through the following equations (Qi et al., 2010):

$$\sigma\ (\mathrm{MPa}) = \frac{P\ (\mathrm{N})}{w\ (\mathrm{mm}) \times d\ (\mathrm{mm})} \quad (1)$$

$$\varepsilon = \frac{l}{l_0} \times 100\% \quad (2)$$

where σ, ε, P, w, d, l, and l_0 stand for stress, strain, load, mat width, mat length, extension length, and gauge length, respectively. Breaking strength, failure strain and Young's modulus can be calculated from stress–strain curves. Note that the area of the fibrous mats is just the effective area of the cross section, and the thickness of the mats was routinely measured using a micrometer and was fixed to be approximately similar (90–100 μm) before measurements.

2.5. Protein adsorption

Protein adsorption onto the electrospun fibrous mats was measured via UV–vis spectrometry. Briefly, the nanofibrous samples assembled with CS/MWCNTs or CS/ALG multilayers (4–8 mg) were cut into a round shape (14 mm in diameter) with a size similar to cover slips, fitted into 24-well cell culture plates, soaked in 75% ethanol for 2 h, and then rinsed three times with phosphate buffered saline (PBS). The wetted scaffolds were exposed to FBS solution (1.5 mL, 10% in PBS buffer) for 24 h in a vapor-bathing constant temperature vibrator at 37 °C (Leong, Chian, Mhaisalkar, Ong, & Ratner, 2009). After incubation, the samples were washed 3 times with PBS buffer (each time with 1 mL PBS buffer for 15 min) to remove the excess protein that was not tightly adsorbed onto the fibrous mats. The washing solution was combined with the FBS solution in PBS buffer after protein adsorption and quantified using a Lambda-25 UV–vis spectrometer (Perkin-Elmer, United States). A standard calibration curve of the absorbance of the FBS at 280 nm as a function of the FBS concentration was used for quantification. Then the amount of protein adsorbed onto the fibrous mats was calculated by subtracting the quantified non-adsorbed protein from the initial total amount of protein.

2.6. In vitro cell culture

L929 cells were cultured in DMEM supplemented with 10% FBS, 100 U/mL penicillin, and 100 U/mL streptomycin. The cell culture was maintained at 37 °C in a humidified incubator with 5% CO_2, and the medium was replaced every 3 d.

To seed cells onto fibrous scaffolds, the polymer nanofibrous mats (14 mm in diameter) were fixed in 24-well cell culture plates with stainless rings and sterilized with 75% alcohol for 2 h, followed by 3 times washing using PBS buffer and overnight soaking in DMEM containing 10% FBS. Then L929 cells were seeded onto the sterilized nanofibrous samples at a density of 2.0×10^4 cells per well. The culture medium was replaced with the new medium every other day.

After being cultured for 3 d, the L929 cells were harvested, rinsed twice with PBS buffer to remove non-adherent cells, and subsequently fixed with 2.5% glutaraldehyde at 4 °C for 2 h. After that, the samples were dehydrated through a series of gradient ethanol solutions of 30%, 50%, 70%, 95%, and 100%, and freeze-dried overnight. Dry samples were sputter coated with a 10 nm-thick gold film before SEM observation of the morphology of cells cultured onto the surface of the scaffolds.

MTT assay was used to quantitatively evaluate the cell viability. Cell attachment assay was performed after seeding cells with a density of 1.5×10^4 cells per well at 1, 2, 4, and 8 h and cell

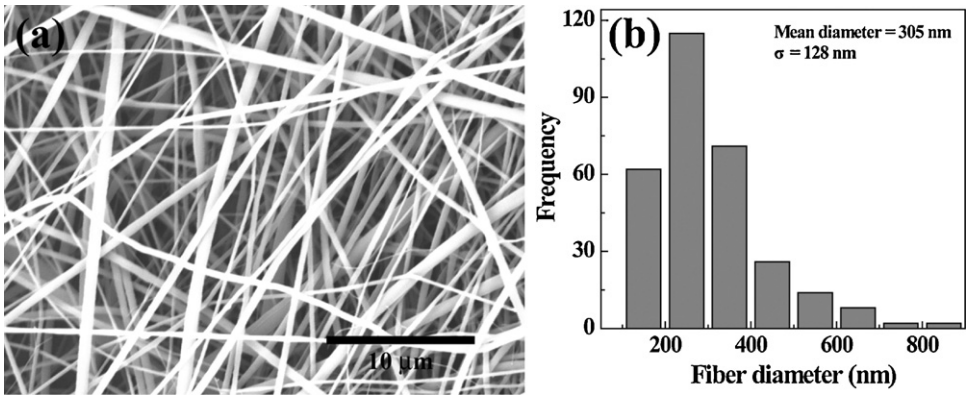

Fig. 2. SEM image and diameter distribution histogram of the CA nanofibrous mats.

proliferation assay was performed after seeding cells with a density of 1.0×10^4 cells per well on days 1, 3, 5, and 7. At each time point, 40 μL MTT solution (C0009, Beyotime Institute of Biotechnology, China) was added to each sample. After 4 h incubation at 37 °C, 400 μL dimethyl sulfoxide (DMSO) was added to dissolve the formazan crystals. Then, the dissolved formazan solution (100 μL) of each sample was added into individual well of a 96-well plate and the absorbance at a wavelength of 570 nm was measured by microplate reader (MK3, Thermo, USA). The absorbance related to the fibrous mats only was corrected to modulate the final optical density (OD) values. Mean and standard deviation for the triplicate wells for each sample were reported.

2.7. Hemocompatibility test

Human red blood cells (HRBCs) were obtained by removing the serum via centrifugation (3000 rpm, 3 min) and washing with PBS buffer according to the procedure reported in literature (Meng, Zheng, Li, & Zheng, 2010). After that, the HRBCs were 10 times diluted with PBS buffer. Then 0.2 mL of the diluted HRBCs suspension was transferred to a 1.5-mL Eppendorf tube which was filled with 0.8 mL of water (as positive control) and PBS buffer (as negative control), respectively. Nanofibrous samples (2 mg) were dipped into 1.0 mL HRBCs suspension containing 0.2 mL diluted HRBCs suspension and 0.8 mL PBS buffer. The above mixtures were then incubated at 37 °C for 60 min, followed by centrifugation (10,000 rpm, 2 min). Then the supernatant was determined by Perkin Elmer Lambda 25 UV–vis spectrometer to record the absorbance at 540 nm. The hemolytic percentage (HP) was calculated using Eq. (3), where D_t is the absorbance of the test samples; D_{pc} and D_{nc} are the absorbance of the positive and negative control, respectively.

$$HP \quad (\%) = \frac{D_t - D_{nc}}{D_{pc} - D_{nc}} \times 100\% \tag{3}$$

2.8. Statistical analysis

The data were expressed as mean ± SD, $n \geq 3$. Statistical analysis was performed by ANOVA method. In all evaluations, $p < 0.05$ was considered as statistically significant.

3. Results and discussion

3.1. Fabrication of CA nanofibers

The CA nanofibers were formed according to the procedures described in our previous work (Xiao et al., 2009). In order to obtain uniform CA nanofibers with a smooth morphology, it is necessary to control the CA concentration in a range of 12–15%. In our study, we chose 12.5% as the optimum concentration of CA for electrospinning. The morphology of the formed nanofibrous mats was observed by SEM (Fig. 2). It is clear that the CA nanofibrous mats display a porous 3D structure with smooth surface and a mean diameter of 305 ± 128 nm. The formed CA mats contain loosely packed fibers, which can be used as templates for multilayer assembly.

3.2. Multilayered assembly of CA nanofibers

The negative surface charge after hydrolysis reaction makes it possible for the CA mats to be assembled with polyelectrolyte multilayers via electrostatic LbL assembly (Wang et al., 2004). To confirm the opposite surface potential of the layering component of CS/MWCNTs and CS/ALG multilayers, the aqueous solutions of CS, MWCNTs, and ALG used for the multilayer deposition onto CA nanofibers were measured by zeta-potential analysis (Table S1, Supplementary Data). It is clear that CS has a potential of +13.8 mV, whereas MWCNTs and ALG have potentials of −20.9 mV and −12.7 mV, respectively. The MWCNTs are able to be well dispersed in water with good colloidal stability, which has been demonstrated in our previous work (Xiao et al., 2010). Therefore, the opposite charge of CS/ALG and CS/MWCNTs pairs should afford the successful electrostatic assembly of the multilayers onto the CA fiber surfaces. We chose the CS as the outmost layer of the multilayer films because CS is positively charged and the surface of cells is negatively charged, which allows efficient cell attachment on the composite multilayered fibrous scaffolds.

The morphology of the multilayered CA $(CS/MWCNTs)_n$ and $CA(CS/ALG)_n$ fibrous scaffolds were observed by SEM. Fig. 3 shows the SEM images of the CA nanofibrous mats coated with 3.5, 5.5, and 10.5 bilayers of CS/ALG and CS/MWCNTs, respectively. With the number of the assembled bilayers, the surfaces of the nanofibers become rougher and rougher, especially for the CS/MWCNTs multilayer-assembled CA nanofibers. It should be noted that the assembly of CS/ALG or CS/MWCNTs multilayers onto each individual CA fiber is likely to be not uniform, since the sites of the tight fiber junction in the inner region of the mats are not able to be assembled. We also note that there is likely a possibility that excess CS is precipitated inside the electrospun mat and trapped in rinsing procedure with water. This leads to a rough surface of CA nanofibers assembled with more bilayers of CS/ALG (Fig. 3c). The much rougher surface of CS/MWCNT multilayered CA mats is likely due to both the deposition of MWCNTs with relatively non-uniform dispersion and the precipitation of excess CS during the rinsing procedure with water. The fiber surface roughness increased substantially as clusters of MWCNTs appear in the SEM images (Fig. 3e and f).

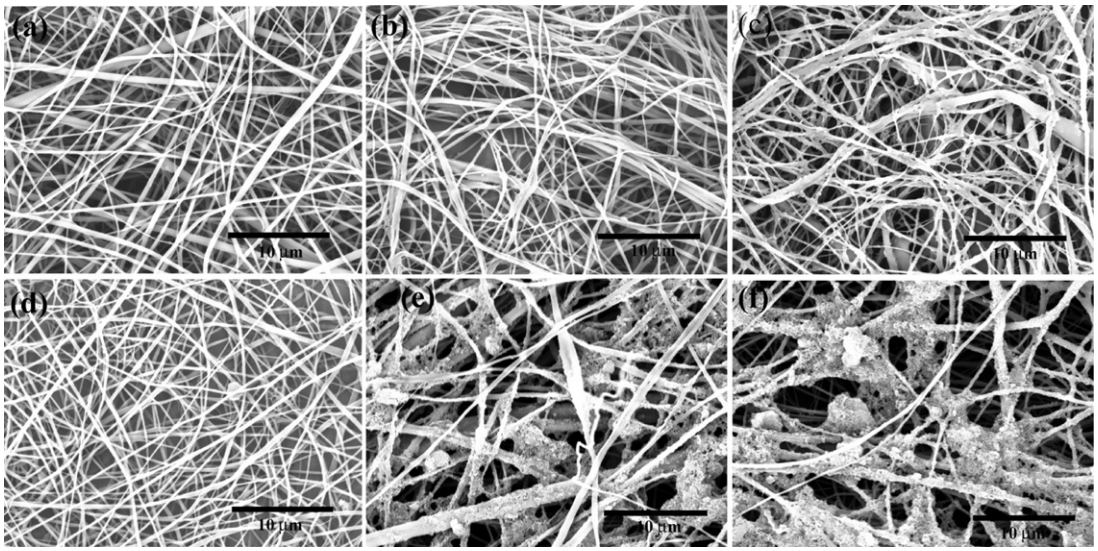

Fig. 3. SEM images of the CA(CS/ALG)$_n$ nanofibers (with n = 3.5 (a), n = 5.5 (b), and n = 10.5 (c), respectively) and CA (CS/MWCNTs)$_n$ nanofibers (with n = 3.5 (d), n = 5.5 (e), and n = 10.5 (f), respectively).

The assembly of both CS/ALG and CS/MWCNTs multilayers onto the CA nanofibers was further characterized by FTIR (Fig. 4). The characteristic bands of CA around 1740 cm^{-1} (C=O) and 1640 cm^{-1} (C—O—O) (Boura et al., 2005) are clear (curve a). After depositing the CS/ALG multilayers, the peak at 3388 cm^{-1} and 2924 cm^{-1} corresponding to the —NH_2 and —CH_2— groups of CS, and the peak at 1602 cm^{-1} belonging to the carboxyl group of ALG can be clearly seen (curve b). For the CS/MWCNTs multilayer-deposited CA nanofibers (curve c), the peaks at 3388 cm^{-1} and 2924 cm^{-1} (—CH_2—) become broad, which is likely due to the strong interaction between the carboxyl residues of MWCNTs and the amino group of CS. The assembly of MWCNTs onto the CA nanofibers was also confirmed by TGA (Supplementary data, Fig. S1). With the 3.5, 5.5, and 10.5 bilayers coating onto the CA nanofibers, the final weight percentage of the residue was calculated to be 17%, 21%, and 27%, respectively, while the weight percentage of the residue is 5% for CA nanofibers without any coatings. The less weight loss at 800 °C with the number of the CS/MWCNTs multilayers clearly suggests the assembly of more MWCNTs on the surface of the CA nanofibers.

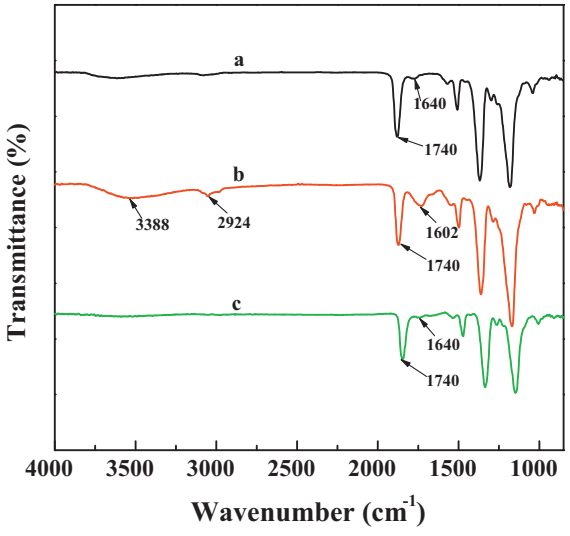

Fig. 4. FTIR spectra of CA (a), CA/(CS/ALG)$_{10.5}$ (b), and CA/(CS/MWCNTs)$_{10.5}$ (c) nanofibrous mats.

We note that the non-linear relationship between the weight loss and the number of MWCNT layers may be due to the non-uniform coating of the MWCNTs after each assembly step. This could particularly happen when the 3D fibrous mats are used as substrates to assemble MWCNTs with relatively non-uniform dispersion when compared with polymers. The combined FTIR and TGA results prove that CS/MWCNTs and CS/ALG multilayers have been successfully assembled on the CA fiber surfaces.

Mechanical durability of electrospun nanofibrous materials is of great importance for their practical applications. The change of the mechanical properties of the CA nanofibrous mats assembled with different bilayers of CS/MWCNTs and CS/ALG was thoroughly investigated. Stress–strain curves of the electrospun composite nanofibrous mats (Fig. S2, Supplementary data) and the detailed mechanical data (Table S2, Supplementary data) clearly show that the CA nanofibers assembled with CS/MWCNTs multilayers display higher tensile stress and ultimate strain when compared with those assembled with similar numbers of CS/ALG multilayers. The enhancement of the mechanical property of the CA/(CS/MWCNTs)$_n$ composite nanofibrous mats should be ascribed to the presence of MWCNTs assembled onto the surface of CA nanofibers, which would allow the load to be efficiently transferred from the CA nanofibrous mats to the MWCNTs that possess extraordinary mechanical properties (Yu et al., 2000). With the number of the deposited CS/MWCNTs bilayers, the tensile stress of the CA nanofibers does not change significantly, while the ultimate strain starts descending, which is probably due to the increased brittleness of the mats with more MWCNTs assembled onto the fiber surfaces. Therefore, less layers of CS/MWCNTs deposition onto the CA nanofibers are beneficial to reserve the improved mechanical property of the nanofibrous scaffold including tensile stress, ultimate strain, and Young's modulus.

3.3. *Protein adsorption onto the multilayered CA nanofibrous scaffolds*

The adsorption of proteins onto artificial tissue engineering scaffolds is an important issue in regulating cellular behavior (Woo, Chen, & Ma, 2003; Woo, Seo, Zhang, & Ma, 2007). It is believed that a scaffold material with more protein adsorption and thus better biocompatibility could better improve the cellular response, enabling enhanced cell adhesion and proliferation

(Lovat et al., 2005; Mattson, Haddon, & Rao, 2000). With the LbL assembly of the defined amount of MWCNTs, it is possible to quantitatively measure the effect of the incorporated MWCNTs on the surface of CA nanofibers on the protein adsorption behavior. Fig. S3 (Supplementary data) shows the amount of protein adsorbed onto the multilayered CA nanofibrous mats after 24 h of incubation in FBS solution. In our experiments, we exposed the nanofibrous mats to 10% FBS in PBS buffer solution in order to simulate the protein adsorption in the cell culture medium, since cell culture medium is quite complex with numerous different components. It is clear that both CS/ALG- and CS/MWCNTs-assembled CA nanofibrous mats are able to absorb much more protein than the cover slips due to their 3D porous fibrous structures with p value less than 0.001 regardless of the number of bilayers. For the CS/MWCNTs-assembled CA nanofibers, deposition of more layers seems to largely improve the protein adsorption ability. For instance, the protein adsorption amount onto the $(CS/MWCNTs)_{10.5}$-assembled CA nanofibers is significantly more than that onto $(CS/ALG)_{10.5}$-assembled CA nanofibers ($P < 0.001$). The protein adsorption capability was further compared using the amount of the protein per milligram of the fibrous mats (Table S3, Supplementary data). Except that the $CA(CS/MWCNTs)_{3.5}$ mat has lower protein adsorption than the $CA(CS/ALG)_{3.5}$ mat, all the CS/MWCNTs-assembled CA nanofibers have better protein

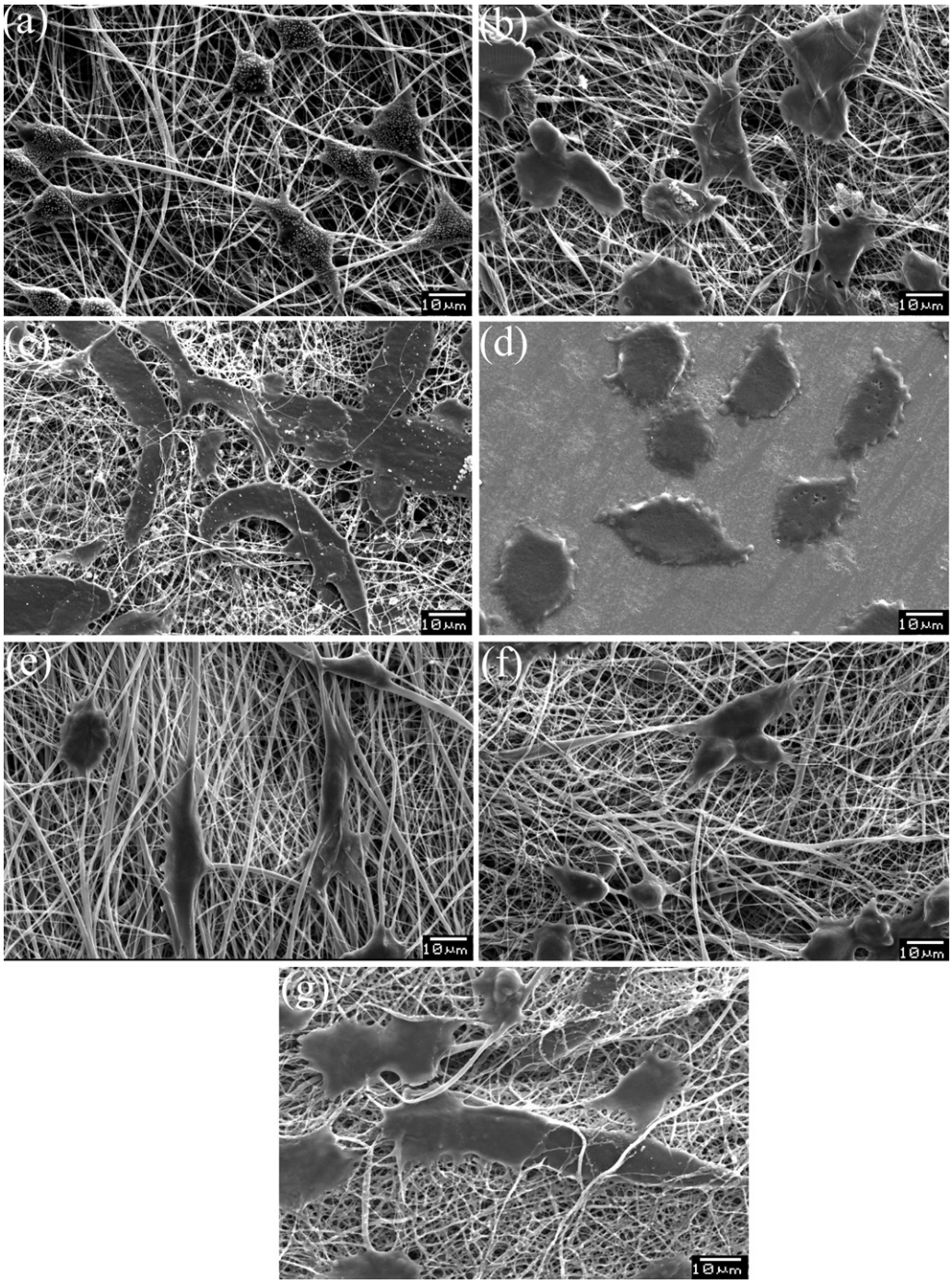

Fig. 5. The morphology of L929 cells cultured onto the $CA/(CS/MWCNTs)_n$ fibrous mats ($n = 3.5$ (a), $n = 5.5$ (b), and $n = 10.5$ (c), respectively) and $CA(CS/ALG)_n$ fibrous mats ($n = 3.5$ (e), $n = 5.5$ (f), and $n = 10.5$ (g), respectively). (d) The control cells cultured onto cover slips.

adsorption capability than the CS/ALG-assembled CA nanofibers with similar numbers of bilayers. This would suggest that the electrospun scaffolds, especially those assembled with more layers of MWCNTs, may provide much higher specific surface area due to the incorporation of hollow cylindrical MWCNTs and/or unique surface features to allow strong interaction with the proteins (Woo et al., 2003). The improved protein adsorption could be due to the electrostatic and/or hydrophobic interaction between MWCNTs and FBS. In addition, the topological features of MWCNTs with high surface area may also facilitate the strong interaction with FBS, in agreement with literature (Chen, Zhang, Wang, & Dai, 2001; Chen et al., 2003; Liao et al., 2011; Meng et al., 2006, 2009). Given the ability of the assembled MWCNTs to improve both the protein adsorption capability and the mechanical durability of the CA nanofibers, the MWCNT-assembled CA nanofibers may hold great promise in tissue engineering applications.

3.4. Morphology and viability assay of cells cultured onto the multilayered CA nanofibrous mats

We next explored the in vitro biocompatibility of multilayered CA nanofibrous scaffolds using L929 cells as a model. The morphology of L929 cells cultured onto cover slips and the multilayered CA nanofibrous mats with different numbers of bilayer deposition and different compositions after 3 d culture was observed by SEM (Fig. 5). It can be seen that the nanofibrous morphology of the multilayered CA scaffolds was well preserved after being soaked in the culture medium for 3 d, and the cells spread and proliferate well on the electrospun nanofibrous substrates. Cells cultured onto all nanofibrous scaffolds regardless of the composition display a phenotypic shape, indicating that the cells can penetrate and migrate within the scaffolds in a manner similar to native ECM. In contrast, cells cultured onto the cover slips display a spindle or asteroid shape (Fig. 5d). For CS/MWCNTs-assembled CA fibrous scaffolds, the cells show asteroid and fusiformate morphology and appear to infiltrate within the porous structure of the nanofibers with the filopodia of the cells closely attached with the nanofibers (Fig. 5a and b), indicating their better cell spreading and proliferation ability than those of the CS/ALG-assembled CA nanofibers.

MTT assay was performed to quantitatively evaluate the viability of cells upon attachment and proliferation onto the different multilayered CA nanofibrous mats. The attachment of L929 cells onto the CS/MWCNTs- and CS/ALG-assembled CA nanofibers was evaluated within a short time period of 8 h (Fig. 6). It is clear that cells cultured onto the $(CS/MWCNTs)_{3.5}$ multilayered scaffolds almost have the best viability at all the time points. For both cases of the multilayered fibrous mats, with the less multilayers coated onto the CA nanofibers, the cells have a better attachment viability. This is likely due to the fact that less layers' coating may maintain well the porous structure of the scaffolds, which is essential for the cell growth. With the same number of multilayer coating, cells cultured onto CS/MWCNTs-coated CA fibers seems to have a better viability than those cultured onto CS/ALG-coated CA fibers.

The biocompatibility of the multilayered CA nanofibrous mats was further evaluated by MTT assay of the viability of cells after seeding on days 1, 3, 5, and 7 (Fig. 7). It can be seen that cells cultured onto the $CA(CS/MWCNTs)_n$ and $CA(CS/ALG)_n$ scaffolds proliferate better than those on the cover slips on days 1 and 5. With the same number of bilayers, there is no distinct difference between the two types of scaffolds with 3.5 and 5.5 bilayers at all 4 time points while $CA(CS/MWCNTs)_{10.5}$ scaffold displays better cell viability than $CA(CS/ALG)_{10.5}$ scaffold with p value <0.05 at all 4 time points. With the more bilayers coated onto the CA nanofibers (e.g., 10.5), the pore volume of the fibrous mats gets smaller, which is not beneficial for the cell growth. However, for the case of the $CA(CS/MWCNTs)_{10.5}$ fibrous mats, the much rougher surface features than that of $CA/(CS/ALG)_{10.5}$ scaffolds along with the good protein adsorption capability of the MWCNTs likely compromise the effect of the low pore volume under similar conditions (Huang et al., 2010).

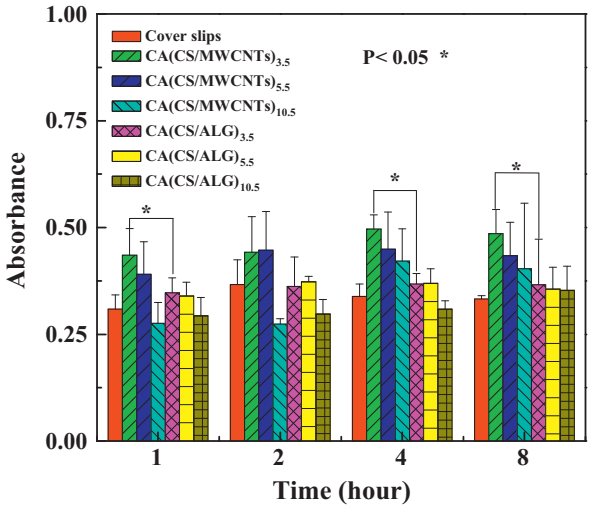

Fig. 6. MTT assay of the adhesion viability of L929 cells seeded onto cover slips (control), $CA/(CS/MWCNTs)_n$, and $CA/(CS/ALG)_n$ nanofibrous mats with $n = 3.5$, 5.5, and 10.5, respectively. The data are expressed as mean ± SD, $n = 3$, the statistical comparisons are made between the $CA/(CS/MWCNTs)_n$ and $CA/(CS/ALG)_n$ nanofibers with similar n and $^{*}p < 0.05$, $^{**}p < 0.01$, $^{***}p < 0.001$.

3.5. Hemocompatibility of the multilayered CA nanofibrous mats

Hemocompatibility is becoming a major concern especially when the developed scaffolds are intended to contact with blood for in vivo applications. Therefore, we explored the hemocompatibility of the CA nanofibers before and after assembly with CS/MWCNTs and CS/ALG multilayers. The HP represents the extent of the HRBCs broken by the sample in contact with blood. As shown in the inset of Fig. 8, no visible hemolytic phenomenon was observed when the fiber mats (2 mg) were exposed to the suspension of the HRBCs. The

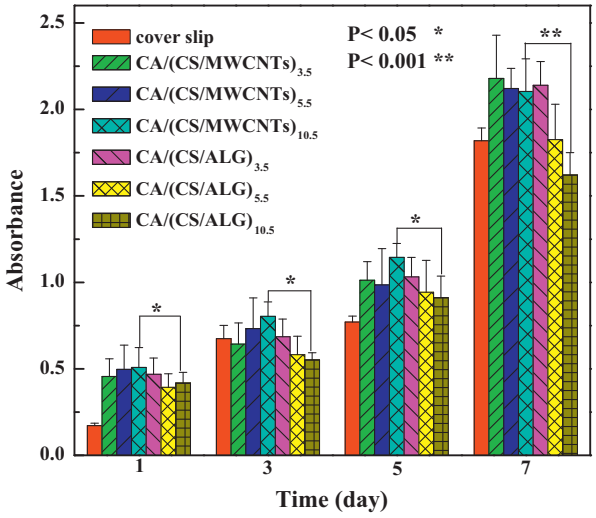

Fig. 7. MTT assay of the proliferation viability of L929 cells seeded onto cover slips (control), $CA/(CS/MWCNTs)_n$, and $CA/(CS/ALG)_n$ nanofibrous mats with $n = 3.5$, 5.5, and 10.5, respectively. The data are expressed as mean ± SD, $n = 3$, the statistical comparisons were made between the $CA/(CS/MWCNTs)_n$ nanofibers and the $CA/(CS/ALG)_n$ nanofibers with similar n and $^{*}p < 0.05$, $^{**}p < 0.01$, $^{***}p < 0.001$.

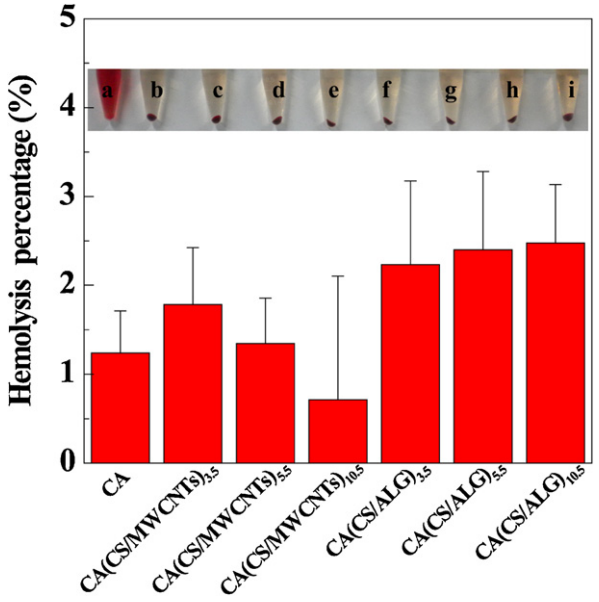

Fig. 8. Hemolysis percentage of the nanofibrous mats before and after assembly. The data are expressed as mean ± SD, $n = 3$, the statistical comparisons were made between the CA/(CS/MWCNTs)$_n$ nanofibers and the CA/(CS/ALG)$_n$ nanofibers with similar n value. The inset shows the solution of HRBCs treated with different nanofiber samples, followed by centrifugation. Samples a–i represent positive control (water), negative control (PBS buffer), CA, CA(CS/MWCNTs)$_{3.5}$, CA(CS/MWCNTs)$_{5.5}$, CA(CS/MWCNTs)$_{10.5}$, CA(CS/ALG)$_{3.5}$, CA(CS/ALG)$_{5.5}$, and CA(CS/ALG)$_{10.5}$ nanofibers, respectively.

measured HPs for all nanofibrous mats were less than 3%, indicating that all of the nanofibrous mats have an excellent hemocompatibility (Wang et al., 2008).

4. Conclusions

In summary, we fabricated both CS/MWCNTs and CS/ALG multilayered CA nanofibrous scaffolds via electrostatic LbL self assembly for tissue engineering applications. The formed multilayered scaffolds were characterized by SEM, FTIR, TGA, and mechanical testing. The CS/MWCNTs multilayer-assembled scaffolds had much rougher surface than that of the CS/ALG multilayered scaffolds with similar number of bilayers. The incorporation of MWCNTs in the multilayered CA fibrous scaffolds tended to enable well attachment, spreading, and proliferation of mouse fibroblast cells when comparing with CS/ALG multilayer-assembled fibrous scaffolds without MWCNTs under the studied conditions. With the good protein adsorption capacity, mechanical durability, cellular attachment and proliferation, and good hemocompatibility, the MWCNTs-containing multilayered composite fibrous scaffolding materials should find applications in tissue engineering and regenerative medicine. The facile LbL self-assembly approach to modifying the nanofibrous scaffolds may be extended for immobilization of other functional bioactive materials for a range of biomedical applications.

Acknowledgements

This research is financially supported by the Key Laboratory of Textile Science & Technology, Ministry of Education, "111 Project", B07024, the National Natural Science Foundation of China (50925312), the Program for New Century Excellent Talents in University, State Education Ministry, and the Science and Technology Collaboration Fund between China and Hungary (No. 5–14), Ministry of Science and Technology. The Shanghai Bai Yu Lan Foundation (11BA1400500) is acknowledged for supporting the collaboration between Donghua University and the University of Madeira. X.S. and H.T. acknowledge FCT for the project PEst-OE/QUI/UI0674/2011 (CQM, Portuguese Government funds). X.S. gratefully acknowledges the Fundação para a Ciência e a Tecnologia (FCT) and Santander bank for the Chair in Nanotechnology. X.C. Thanks the financial support from the Key Laboratory of Science & Technology of Eco-Textile (Donghua University/Jiangnan University), Ministry of Education.

Appendix A. Supplementary data

Supplementary data associated with this article can be found, in the online version, at http://dx.doi.org/10.1016/j.carbpol.2012.08.069.

References

Abraham, S., Riggs, M. J., Nelson, K., Lee, V., & Rao, R. R. (2010). Characterization of human fibroblast-derived extracellular matrix components for human pluripotent stem cell propagation. *Acta Biomaterialia*, *6*(12), 4622–4633.

Almodóvar, J., & Kipper, M. J. (2011). Coating electrospun chitosan nanofibers with polyelectrolyte multilayers using the polysaccharides heparin and N,N,N-trimethyl chitosan. *Macromolecular Bioscience*, *11*(1), 72–76.

Bhattarai, N., Li, Z., Edmondson, D., & Zhang, M. (2006). Alginate-based nanofibrous scaffolds: Structural, mechanical, and biological properties. *Advanced Materials*, *18*(11), 1463–1467.

Boura, C., Muller, S., Vautier, D., Dumas, D., Schaaf, P., V, J., et al. (2005). Endothelial cell – interactions with polyelectrolyte multilayer films. *Biomaterials*, *26*(22), 4568–4575.

Chen, R. J., Bangsaruntip, S., Drouvalakis, K. A., Wong Shi Kam, N., Shim, M., Li, Y., et al. (2003). Noncovalent functionalization of carbon nanotubes for highly specific electronic biosensors. *Proceedings of the National Academy of Sciences of the United States of America*, *100*(9), 4984–4989.

Chen, R. J., Zhang, Y., Wang, D., & Dai, H. (2001). Noncovalent sidewall functionalization of single-walled carbon nanotubes for protein immobilization. *Journal of the American Chemical Society*, *123*(16), 3838–3839.

Chicatun, F., Pedraza, C. E., Ghezzi, C. E., Marelli, B., Kaartinen, M. T., McKee, M. D., et al. (2011). Osteoid-mimicking dense collagen/chitosan hybrid gels. *Biomacromolecules*, *12*, 2946–2956.

Decher, G. (1997). Fuzzy nanoassemblies: Toward layered polymeric multicomposites. *Science*, *277*(5330), 1232–1237.

Deng, H., Wang, X., Liu, P., Ding, B., Du, Y., Li, G., et al. (2011). Enhanced bacterial inhibition activity of layer-by-layer structured polysaccharide film-coated cellulose nanofibrous mats via addition of layered silicate. *Carbohydrate Polymers*, *83*(1), 239–245.

Deng, H., Zhou, X., Wang, X., Zhang, C., Ding, B., Zhang, Q., et al. (2010). Layer-by-layer structured polysaccharides film-coated cellulose nanofibrous mats for cell culture. *Carbohydrate Polymers*, *80*(2), 474–479.

Halthur, T. J., & Elofsson, U. M. (2004). Multilayers of charged polypeptides as studied by in situ ellipsometry and quartz crystal microbalance with dissipation. *Langmuir*, *20*(5), 1739–1745.

Harrington, D. A., Cheng, E. Y., Guler, M. O., Lee, L. K., Donovan, J. L., Claussen, R. C., et al. (2006). Branched peptide-amphiphiles as self-assembling coatings for tissue engineering scaffolds. *Journal of Biomedical Materials Research Part A*, *78*(1), 157–167.

Huang, C., Chen, R., Ke, Q., Morsi, Y., Zhang, K., & Mo, X. (2010). Electrospun collagen–chitosan–TPU nanofibrous scaffolds for tissue engineered tubular grafts. *Colloids and Surfaces B: Biointerfaces*, *82*(2), 307–315.

Kinnane, C. R., Wark, K., Such, G. K., Johnston, A. P. R., & Caruso, F. (2009). Peptide-functionalized, low-biofouling click multilayers for promoting cell adhesion and growth. *Small*, *5*(4), 444–448.

Langer, R. S., & Vacanti, J. P. (1993). Tissue engineering. *Science*, *260*(5110), 920–926.

Langer, R. S., & Vacanti, J. P. (1999). Tissue engineering: The challenges ahead. *Scientific American*, *280*(4), 86–89.

Lavalle, P., Gergely, C., Cuisinier, F. J. G., Decher, G., Schaaf, P., Voegel, J. C., et al. (2002). Comparison of the structure of polyelectrolyte multilayer films exhibiting a linear and an exponential growth regime: An in situ atomic force microscopy study. *Macromolecules*, *35*(11), 4458–4465.

Leong, M., Chian, K., Mhaisalkar, P., Ong, W., & Ratner, B. (2009). Effect of electrospun poly(D,L-lactide) fibrous scaffold with nanoporous surface on attachment of porcine esophageal epithelial cells and protein adsorption. *Journal of Biomedical Materials Research Part A*, *89A*(4), 1040–1048.

Li, M., Mondrinos, M. J., Gandhi, M. R., Ko, F. K., Weiss, A. S., & Lelkes, P. I. (2005). Electrospun protein fibers as matrices for tissue engineering. *Biomaterials*, *26*(30), 5999–6008.

Li, W. J., Laurencin, C. T., Caterson, E. J., Tuan, R. S., & Ko, F. K. (2002). Electrospun nanofibrous structure: A novel scaffold for tissue engineering. *Journal of Biomedical Materials Research*, *60*(4), 613–621.

Liao, H., Qi, R., Shen, M., Cao, X., Guo, R., Zhang, Y., et al. (2011). Improved cellular response on multiwalled carbon nanotube-incorporated electrospun polyvinyl

alcohol/chitosan nanofibrous scaffolds. *Colloids and Surfaces B: Biointerfaces*, *84*(2), 528–535.
Liu, F., Guo, R., Shen, M., Cao, X., Mo, X., Wang, S. H., et al. (2010). Effect of the porous microstructures of poly (lactic-co-glycolic acid)/carbon nanotube composites on the growth of fibroblast cells. *Soft Materials*, *8*(3), 239–253.
Liu, F., Guo, R., Shen, M., Wang, S. H., & Shi, X. (2009). Effect of processing variables on the morphology of electrospun poly [(lactic acid)-co-(glycolic acid)] nanofibers. *Macromolecular Materials and Engineering*, *294*(10), 666–672.
Lovat, V., Pantarotto, D., Lagostena, L., Cacciari, B., Grandolfo, M., Righi, M., et al. (2005). Carbon nanotube substrates boost neuronal electrical signaling. *Nano Letters*, *5*(6), 1107–1110.
Lu, X., & Imae, T. (2007). Size-controlled in situ synthesis of metal nanoparticles on dendrimer-modified carbon nanotubes. *The Journal of Physical Chemistry C*, *111*(6), 2416–2420.
Mamedov, A. A., & Kotov, N. A. (2000). Free-standing layer-by-layer assembled films of magnetite nanoparticles. *Langmuir*, *16*(13), 5530–5533.
Mattson, M. P., Haddon, R. C., & Rao, A. M. (2000). Molecular functionalization of carbon nanotubes and use as substrates for neuronal growth. *Journal of Molecular Neuroscience*, *14*(3), 175–182.
Meng, J., Kong, H., Han, Z., Wang, C., Zhu, G., Xie, S., et al. (2009). Enhancement of nanofibrous scaffold of multiwalled carbon nanotubes/polyurethane composite to the fibroblasts growth and biosynthesis. *Journal of Biomedical Materials Research Part A*, *88*(1), 105–116.
Meng, J., Song, L., Kong, H., Zhu, G., Wang, C., Xu, L., et al. (2006). Using single-walled carbon nanotubes nonwoven films as scaffolds to enhance long-term cell proliferation in vitro. *Journal of Biomedical Materials Research Part A*, *79*(2), 298–306.
Meng, Z. X., Zheng, W., Li, L., & Zheng, Y. F. (2010). Fabrication and characterization of three-dimensional nanofiber membrance of PCL-MWCNTs by electrospinning. *Materials Science and Engineering: C*, *30*(7), 1014–1021.
Mo, X. M., Xu, C. Y., Kotaki, M., & Ramakrishna, S. (2004). Electrospun P (LLA-CL) nanofiber: A biomimetic extracellular matrix for smooth muscle cell and endothelial cell proliferation. *Biomaterials*, *25*(10), 1883–1890.
Olek, M., Ostrander, J., Jurga, S., Möhwald, H., Kotov, N., Kempa, K., et al. (2004). Layer-by-layer assembled composites from multiwall carbon nanotubes with different morphologies. *Nano Letters*, *4*(10), 1889–1895.
Petersen, E. J., Huang, Q., & Weber, W. J., Jr. (2008). Ecological uptake and depuration of carbon nanotubes by Lumbriculus variegatus. *Environmental Health Perspectives*, *116*(4), 496.
Picart, C., Elkaim, R., Richert, L., Audoin, F., Arntz, Y., Da Silva Cardoso, M., et al. (2005). Primary cell adhesion on RGD-functionalized and covalently crosslinked thin polyelectrolyte multilayer films. *Advanced Functional Materials*, *15*(1), 83–94.
Qi, R., Guo, R., Shen, M., Cao, X., Zhang, L., Xu, J., et al. (2010). Electrospun poly (lactic-co-glycolic acid)/halloysite nanotube composite nanofibers for drug encapsulation and sustained release. *J. Mater. Chem.*, *20*(47), 10622–10629.
Reneker, D. H., & Chun, I. (1996). Nanometre diameter fibres of polymer, produced by electrospinning. *Nanotechnology*, *7*, 216–223.
Rodríguez, K., Renneckar, S., & Gatenholm, P. (2011). Biomimetic calcium phosphate crystal mineralization on electrospun cellulose-based scaffolds. *ACS Applied Materials & Interfaces*, *3*(3), 681–689.
Rowley, J. A., Madlambayan, G., & Mooney, D. J. (1999). Alginate hydrogels as synthetic extracellular matrix materials. *Biomaterials*, *20*(1), 45–53.
Schlenoff, J. B., & Decher, G. (2003). *Multilayer thin films: Sequential assembly of nanocomposite materials*. Weinheim, Germany: Wiley, VCH.
Sottile, J. (2004). Regulation of angiogenesis by extracellular matrix. *Biochimica et Biophysica Acta (BBA) – Reviews on Cancer*, *1654*(1), 13–22.
Wang, Q. Z., Chen, X. G., Li, Z. X., Wang, S., Liu, C. S., Meng, X. H., et al. (2008). Preparation and blood coagulation evaluation of chitosan microspheres. *J. Mater. Sci. – Mater. Med.*, *19*(3), 1371–1377.
Wang, X., Kim, Y. G., Drew, C., Ku, B. C., Kumar, J., & Samuelson, L. A. (2004). Electrostatic assembly of conjugated polymer thin layers on electrospun nanofibrous membranes for biosensors. *Nano Letters*, *4*(2), 331–334.
Wei, G., & Ma, P. X. (2008). Nanostructured biomaterials for regeneration. *Advanced Functional Materials*, *18*(22), 3568–3582.
Woo, K. M., Chen, V. J., & Ma, P. X. (2003). Nano-fibrous scaffolding architecture selectively enhances protein adsorption contributing to cell attachment. *Journal of Biomedical Materials Research Part A*, *67*(2), 531–537.
Woo, K. M., Seo, J., Zhang, R., & Ma, P. X. (2007). Suppression of apoptosis by enhanced protein adsorption on polymer/hydroxyapatite composite scaffolds. *Biomaterials*, *28*(16), 2622–2630.
Xiao, S., Shen, M., Guo, R., Huang, Q., Wang, S., & Shi, X. (2010). Fabrication of multi-walled carbon nanotube-reinforced electrospun polymer nanofibers containing zero-valent iron nanoparticles for environmental applications. *Journal of Materials Chemistry*, *20*(27), 5700–5708.
Xiao, S., Wu, S., Shen, M., Guo, R., Huang, Q., Wang, S., et al. (2009). Polyelectrolyte multilayer-assisted immobilization of zero-valent iron nanoparticles onto polymer nanofibers for potential environmental applications. *ACS Applied Materials & Interfaces*, *1*(12), 2848–2855.
Yang, S. Y., Mendelsohn, J. D., & Rubner, M. F. (2003). New class of ultrathin, highly cell-adhesion-resistant polyelectrolyte multilayers with micropatterning capabilities. *Biomacromolecules*, *4*(4), 987–994.
Yoshimoto, H., Shin, Y. M., Terai, H., & Vacanti, J. P. (2003). A biodegradable nanofiber scaffold by electrospinning and its potential for bone tissue engineering. *Biomaterials*, *24*(12), 2077–2082.
Yu, M. F., Lourie, O., Dyer, M. J., Moloni, K., Kelly, T. F., & Ruoff, R. S. (2000). Strength and breaking mechanism of multiwalled carbon nanotubes under tensile load. *Science*, *287*(5453), 637–640.
Zhou, H., & Xu, H. H. K. (2011). The fast release of stem cells from alginate-fibrin microbeads in injectable scaffolds for bone tissue engineering. *Biomaterials*, *32*, 7503–7513.